Low-carbon Operation of Combined Heat and Power Integrated Plants Based on Solar-assisted Carbon Capture

Xusheng Guo, Suhua Lou, Yaowu Wu, and Yongcan Wang

***Abstract*—Accelerating the development of renewable energy and reducing CO_2 emissions have become a general consensus and concerted action of all countries in the world. The electric power industry, especially thermal power industry, is the main source for fossil energy consumption and CO_2 emissions. Since solvent-based post-combustion carbon capture technology would bring massive extra energy consumption, the application of solar-assisted carbon capture technology has attracted extensive attention. Due to the important role of coal-fired combined heat and power plants for serving residential and industrial heating districts, in this paper, the low-carbon operation benefits of combined heat and power integrated plants based on solar-assisted carbon capture (CHPIP-SACC) are fully evaluated in heat and power integrated energy system with a high proportion of wind power. Based on the selected integration scheme, a linear operation model of CHPIP-SACC is developed considering energy flow characteristics and thermal coupling interaction of its internal modules. From the perspective of system-level operation optimization, the day-ahead economic dispatch problem based on a mix-integer linear programming model is presented to evaluate the low-carbon benefits of CHPIP-SACC during annual operation simulation. The numerical simulations on a modified IEEE 39-bus system demonstrate the effectiveness of CHPIP-SACC for reducing CO_2 emissions as well as increasing the downward flexibility. The impact of different solar field areas and unit prices of coal on the low-carbon operation benefits of CHPIP-SACC is studied in the section of sensitivity analysis.**

***Index Terms*—Solar-assisted carbon capture, CO_2 emission reduction, combined heat and power integrated plant, heat and power integrated energy system, wind power.**

NOMENCLATURE

A. Indices and Sets

Ω	Set of scenarios
d	Index of days
f	Index of wind farms
F	Set of wind farms
g	Index of CHP units
G	Set of combined heat and power (CHP) units
h	Index of load nodes
i, j	Index of bus nodes
I, R	Sets of CHP units supplying heat for industrial and residential areas
s	Index of seasons
t	Index of time nodes
T	Set of time periods

B. Parameters and Constants

Δt	Unit time interval
$\beta^{C}_{\max}$	The maximum carbon capture rate
η^{coal}	Combustion efficiency of pulverized coal in the boiler
η_{CO_2}	Mass ratio of CO_2 that can be sold to industry to the total CO_2 captured
η^{c}, η^{d}	Charging and discharging efficiencies of thermal storage module
$\eta^{h,e}$	Thermo-electric conversion efficiency of steam-cogeneration module under pure condensing condition
η^{sf}	Photo-thermal comprehensive conversion efficiency
λ_C	Carbon trading price per unit mass of CO_2
λ_{CO_2}	Sale price per unit mass of captured CO_2 used for industry
λ^{coal}	Purchase price per unit mass of thermal coal
$\mu^{bc,in}$	Coefficient to limit the output power of regenerative heating module based on input power of boiler combustion module
$\mu^{bc,out}$	Coefficient to limit thermal power of extraction steam from each stage of turbine based on output power of boiler

Manuscript received: January 21, 2021; revised: May 9, 2021; accepted: September 22, 2021. Date of CrossCheck: September 22, 2021. Date of online publication: November 24, 2021.

This work was supported in part by the National Natural Science Foundation of China (No. 51977087), and in part by the Science and Technology Project of State Grid Corporation of China (No. 1400-202199550A-0-5-ZN).

X. Guo, S. Lou (corresponding author), Y. Wu, and Y. Wang are with the State Key Laboratory of Advanced Electromagnetic Engineering and Technology, Huazhong University of Science and Technology, Wuhan 430074, China, and Y. Wang is also with State Grid Sichuan Electric Power Research Institute, Chengdu 610041, China (e-mail: xushengguo@hust.edu.cn; shlou@mail.hust.edu.cn; ywwu@hust.edu.cn; wangyc@hust.edu.cn).

DOI: 10.35833/MPCE.2021.000046

$\mu^{ex}_{\min}$, $\mu^{ex}_{\max}$ Coefficients that determine the minimum and maximum thermal power of exhausted steam that has done work in steam turbine

π_s Number of days in the season of scenario s

$\varphi_{l,e,cur}$, $\varphi_{l,h,cur}$ Penalty coefficients for electric and thermal load sheddings

$\varphi_{res,cur+}$ Penalty coefficient for insufficient positive reserve

$\varphi_{res,cur-}$ Penalty coefficient for insufficient negative reserve

$\varphi_{s,cur}$, $\varphi_{w,cur}$ Penalty coefficients for solar and wind curtailments

c_m Slope of working condition line related to the minimum condensing steam

c_v Slope of working condition line related to extraction steam for supplying heat

C^B_g Basic fixed operating and maintenance cost of CHP unit g

e^C Mass of CO_2 emitted by combusting per unit mass of pulverized coal

ET_0, ET_T Thermal storage energy levels at initial time and time T

$ET_{\min}$, $ET_{\max}$ The minimum and maximum thermal storage capacities

$M_{\min}$, $M_{\max}$ The minimum and maximum masses of pulverized coal combusted per unit time in the boiler

p^C Thermal power consumed to capture per unit mass of CO_2 per unit time

p_s Probability of scenario s

$PC^{op}_{\max}$ The maximum operation power of carbon capture module

$PH^{net}_{\min}$, $PH^{net}_{\max}$ The minimum and maximum net thermal power used by steam turbine

$PT^c_{\max}$, $PT^d_{\max}$ The maximum charging and discharging power of thermal storage

$P^{l,e}_{s,i,t}$ Electric load of node i at time t in scenario s

$P^{l,h,r}_{s,t}$, $P^{l,h,i}_{s,t}$ Thermal loads of residential and industrial heating areas at time t in scenario s

q As-received basis net calorific value of pulverized coal

$r^{down}_{\max}$, $r^{up}_{\max}$ The maximum ramp-down and ramp-up rates in boiler combustion module

S^{sf} Area of solar field

C. Variables

β^C_t Carbon capture rate at time t, which denotes the mass ratio of captured CO_2 to the total CO_2 produced by boiler combustion module

$\theta_{s,i,t}$, $\theta_{s,j,t}$ Voltage phases of nodes i and j at time t in scenario s

ET_t Existing thermal storage capacity level at time t

M_t Mass of pulverized coal combusted per unit time interval at time t

PB^{in}_t Input power generated by combusting pulverized coal in the boiler at time t

PB^{out}_t Output power of boiler combustion module at time t, which denotes thermal power of the main steam generated by the boiler

PC^B Basic and fixed operating power consumption of carbon capture module

PC^{in}_t Input power of carbon capture module directly provided by solar collector module at time t, which forms part of its operation power

PC^{op}_t Operation power of carbon capture module at time t

PH^{net}_t Net thermal power used by steam turbine at time t

PR^{in}_t Input power of regenerative heating module at time t, which denotes the thermal power of extraction steam from each stage of turbine

PR^{ex}_t Thermal power of exhausted steam that has done work in steam turbine at time t

PR^{out}_t Output power of regenerative heating module at time t, which denotes preheating power of feed water

PS^{in}_t Real input thermal power generated by solar collector module considering solar curtailment at time t

$PT^{c,pr}_t$, $PT^{c,ps}_t$ Charging power of thermal storage from regenerative heating module and solar collector module

$PT^{d,pr}_t$, $PT^{d,pc}_t$ Discharging power of thermal storage to regenerative heating and carbon capture modules

P^{sf}_t Available heat collection power produced by solar concentration at time t

P^{ConP}_t Electric output power of CHP unit under pure condensing condition at time t

P^{ExP}_t, P^{ExH}_t Output power of electricity and heat of CHP unit under extraction condition at time t

P^{ExH}_0 Intersection of the minimum condensing working condition line with x-axis

$P^{l,e,cur}_{s,t}$ Electric load shedding at time t in scenario s

$P^{sp}_{s,i,t}$ Injected power of node i at time t in scenario s

$P_{s,ij,t}$ Line transmission power from node i to node j at time t in scenario s

$P^{w,f}_{s,f,t}$, $P^{w,e}_{s,f,t}$ Available and grid-connected wind power of wind farm f at time t in scenario s

$P^{l,h,r,cur}_{s,t}$ Thermal load shedding of residential heating area at time t in scenario s

$P^{l,h,i,cur}_{s,t}$ Thermal load shedding of industrial heating area at time t in scenario s

R^{sf}_t Direct normal irradiance at time t, which represents vertically radiated solar power per unit area

$R^{res,cur+}_{s,t}$ Number of insufficient positive reserve capacity at time t in scenario s

$R_{s,t}^{res,cur-}$ Number of insufficient negative reserve capacity at time t in scenario s

$R_{s,t}^{res,D+}$, $R_{s,t}^{res,D-}$ Positive and negative reserve demands at time t in scenario s

$R_{s,t}^{res,S+}$, $R_{s,t}^{res,S-}$ Positive and negative reserve supplies at time t in scenario s

$z_t^{op,pc}$ Operation state indicator for the carbon capture module at time t, equal to 1 if the carbon capture module is at operation state and 0 otherwise

$z_t^{c,pr}$, $z_t^{c,ps}$ Charging state indicators for thermal storage charging from regenerative heating and solar collector modules at time t, equal to 1 if thermal storage is at charging state and 0 otherwise

$z_t^{d,pr}$, $z_t^{d,pc}$ Discharging state indicators for thermal storage discharging to regenerative heating and carbon capture modules at time t, equal to 1 if thermal storage is at discharging state and 0 otherwise

I. Introduction

With the increasingly serious fossil energy shortage, global warming and deterioration of ecological environment, it has become a general consensus and concerted action of all countries in the world to accelerate the development of renewable energy and reduce carbon emissions [1]-[4]. As an international legal milestone document in human history to deal with climate change, Paris Agreement clarifies the goal of achieving global balance between greenhouse gas emissions and its absorptions in the second half of this century. China hopes to work with other countries to jointly promote low-carbon sustainable development [5], so as to build a community of shared future for mankind and achieve win-win cooperation. China has promised that it would adopt stronger policies and measures to strive to reach the peak of carbon emissions before 2030 and try its best to achieve carbon neutrality before 2060.

The electric power industry, especially thermal power industry, is the main source for fossil energy consumption and CO_2 emissions. In 2018, the global CO_2 emissions reached a record of 33.1 billion tons, of which the electric power industry accounted for 38% [6]. In order to achieve the targets related to CO_2 emission reduction, it is necessary to realize the renewable-energy-dominated electric energy supply structure so as to carry out the green transition of electric energy.

However, for many developing countries, limited by scarce and expensive natural gas resources, coal-fired thermal power plants account for a large proportion of installed capacity over a long time. For example, in 2018, the coal-fired units in China, South Africa, and India accounted for 66.5%, 87.9%, and 75.4% of their own total installed capacity, while the gas-fired units only accounted for 3.2%, 0.7% and 4.8%, respectively [7]. Since the existing coal-fired units still have a long service life and are difficult to be completely replaced in a short term, a large amount of CO_2 emissions would be generated during their operation [8]. In particular, in some areas such as Three Northern Areas of China, a large number of combined heat and power (CHP) generations are operated to supply heat for residential and industrial uses, which account for more than half of the thermal power units [9]-[11]. This leads to serious problems of CO_2 emissions, especially in peak heating season such as winter [12]. These situations have brought severe challenges to the transition towards clean and low-carbon energy systems.

In response to the above problems, two feasible solutions have been proposed: ① add carbon capture, utilization and storage (CCUS) devices by retrofitting coal-fired power plants; ② adjust the role of coal-fired power plants so that more reserve capacity and flexibility can be provided for power system while the utilization hours of them can be reduced. At present, in the field of power system operation optimization, extensive and deep studies have been conducted on how to use CCUS technology to jointly realize the above two solutions. Due to the ease of retrofitting, as one of mature and promising technologies, solvent-based post-combustion carbon capture is mainly used in [13], [14]. However, since the CO_2 desorption and absorbent regeneration process requires massive energy consumption, the actual output power of coal-fired power units would be reduced significantly unless their original output power is maintained at the expense of greatly increasing their coal consumption rate [15]-[17]. For example, it is shown that after installing carbon capture systems, the actual output power of 600 MW and 320 MW units has been reduced by 12.4% and 16%, respectively [18], [19]. This problem hinders the large-scale application of carbon capture technology.

Recently, in order to avoid the massive energy consumption caused by carbon capture, adopting solar thermal energy as an external heat source for assisting carbon capture instead of only utilizing extraction steam from internal coal-fired units has attracted extensive research attention, which is called solar-assisted carbon capture (SACC) technology. Compared with concentrating solar plants (CSPs) and the embryonic form of solar-assisted coal-fired power generation, the solar field area required by the proposed technology is much smaller.

In the view of technical feasibility including internal operation principle and reasonable integration schemes, [20] reviews the existing studies on the utilization of SACC in assisting coal-fired power plants. Based on some mature integration schemes and equipment options, the technical characteristics and energy coupling relationship of internal modules are illustrated in detail. Reference [21] establishes matrix models to comprehensively investigate the thermal performance such as external fuel exergy contribution of two representative integration schemes of coal-fired thermal power plants based on SACC. Reference [22] builds a pilot system of SACC to compare the performance of two types of solar thermal energy collectors, i. e., parabolic trough collector (PTC) and linear Fresnel reflector (LFR). It is found that both PTC and LFR can fully provide the heat energy required by the reboilers of carbon capture system. The efficiency of PTC is better than that of LFR, and the former is also less sensitive to direct normal irradiance (DNI) of solar energy. Reference [23] systematically evaluates and com-

pares the thermodynamic processes such as chemical reactions and operating conditions among different novel SACC technologies. After calculating the performance evaluation indicators such as the second-law efficiency, some novel technical routes have been pointed out to be more mature and promising with relatively higher energy efficiencies, while some technical routes are the opposite.

As for the economic feasibility including the levelized cost of electricity (LCOE) and the investment cost, based on a micro-turbine cogeneration system installed in Cuernavaca, Mexico, [24] demonstrates that the use of solar energy would help increase the efficiency of the cogeneration system when coupled with post-combustion carbon capture. This technology would help realize the near-zero carbon emissions of cogeneration system, but it would also cause a substantial increase in LCOE. Thus, it is necessary for the government to formulate effective incentive policies about carbon emission reduction to promote the development of this technology. Based on the parameters of a 300 MW coal-fired thermal power plants in New South Wales, Australia, as well as the local data of electricity price and the weather, [25] demonstrates the techno-economic of SACC through evaluating the impact of solar collector cost, carbon price, and solar load fraction on the net revenue of retrofitted thermal power plants. The results point out the range of each influencing factor to make the proposed technology economically viable. Reference [26] calculates the net annual revenue of coal-fired power plants after integrating SACC considering different incentives, e.g., preferential discount rates, subsidies, carbon tax and renewable energy certificates.

In summary, based on the pilot equipment or exergy matrix models, the thermal performance such as thermal efficiency and thermal economy has been analyzed to illustrate the technical feasibility of the proposed technology. Based on economic parameters and incentive policies, the net revenue from the perspective of a single equipment itself has been calculated to demonstrate its economic feasibility. However, the existing studies rarely focus on the annual operation benefits of this promising technology from the perspective of overall power system, especially with high share of stochastic wind power output. Considering the computational complexity, the above research with physical test or thermodynamic model cannot be suitable for solving the problems of operation scheduling and benefit evaluation in power system after adopting SACC. Therefore, after making a trade-off between computational efficiency and analytical accuracy, a new operation model of retrofitted thermal power units based on SACC should be established.

As for the modeling issues for retrofitted thermal power plants, [8] establishes an operation model about retrofitted conventional coal-fired thermal power plants that can only produce electricity. Compared with the previous operation models of electric output and fuel consumption based on simple quadratic functions, the internal systems such as boiler combustion system and steam turbine system have been considered as relatively separate input and output modules more precisely. This model is not only suitable for power system scheduling and benefit evaluation, but also capable of reflecting their internal thermal coupling relationship and energy flow characteristics. However, only the flexibility retrofit for conventional thermal power plants has been considered, while the retrofit technology related to carbon emission reduction is not. Therefore, a new input and output modules of SACC system are designed, proposed, and integrated on thermal power units. Considering that the CHP units are widely used for serving residential areas and industrial parks, we extend the operation model of conventional coal-fired thermal power units to CHP units. In addition, compared with the previous thermal power model, the roles of the regenerative heating system and thermal storage system in the internal thermal power units are also further developed.

Therefore, based on the above discussion, we focus on fully evaluating the annual low-carbon operation benefits of combined heat and power integrated plants (CHPIPs) installed with SACC systems from the perspective of power and heat integrated energy system (PHIES) with a high proportion of wind power. The contribution of this paper can be summarized as follows.

1) To describe its thermal energy coupling and energy flow characteristics, a linear operation model of CHPIP-SACC is developed, which is suitable for operation optimization at system level.

2) To evaluate the low-carbon benefits of CHPIP-SACC in PHIES during annual operation simulation, the day-ahead economic dispatch problem is presented based on a mix-integer linear programming model, which can also fully measure the positive and negative reserve capacity of CHPIPs.

3) To further illustrate the impact of different solar field areas and different unit prices of coal on annual operation benefits of CHPIPs in PHIES, sensitivity analysis is performed in numerical simulations.

The remainder of this paper is organized as follows. Section II integrates SACC system in CHPIPs, where a linear operation model of CHPIPs is developed after selecting a mature integration scheme and analyzing their internal energy flow process. The day-ahead economic dispatch problem used to evaluate the low-carbon benefit of CHPIPs during annual operation simulation is presented in Section III. A case study is performed in Section IV, whose results have also been illustrated and analyzed. The conclusion and the outlook are shown in Section V.

II. Integrating SACC System in CHPIPs

A. Basic Principles and Integration Scheme for SACC

Considering the technologies that have achieved mature commercial applications, PTC [22] and post-combustion carbon capture based on chemical absorption and molten-salt thermal storage [27] are selected as the modules for the integration of SACC system. When SACC system is integrated into CHP units, it is necessary to ensure that the operating temperature of each module is relatively matched. Therefore, the working fluid, i.e., water, is used as a medium for the exchange of material flow and energy flow. Based on previous research [20], [21], [25], the selected structure diagram of

CHPIP-SACC is shown in Fig. 1. It can be observed from Fig. 1 that the condensate coming from the condenser is divided into two parts. One part continues to be heated by low-pressure (LP) and high-pressure (HP) heaters in regenerative heating module. The other part is firstly heated by solar collector module and then provides heat energy for rich liquid regeneration process of the carbon capture module, the excessive thermal energy of which would be stored in thermal storage module. Finally, the return water is sent to the outlet of a certain stage heater. In Fig. 1, IP, LT, and HT represent intermediate pressure, low temperature, and high temperature, respectively.

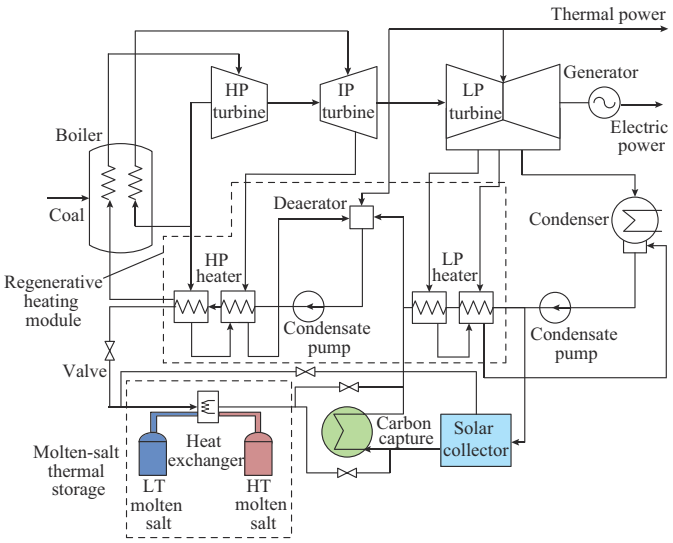

Fig. 1. Structure diagram of CHPIP-SACC.

The thermal storage module, which is tightly coupled with the regenerative heating module, plays an important role as a bridge to constitute the interaction between the SACC subsystem and the original CHP sub-system. It is not only a back-up heat source for carbon capture, but also able to release thermal energy to heat feed water of regenerative heating module, which can reduce the coal consumption rate and operation cost of CHP units. Moreover, when the electric load is low but the wind power is high, more steam can be extracted from each stage of steam turbine, whose thermal energy can be stored in thermal storage module through heat exchanger. This can reduce the minimum technical electric output of the CHP units, so as to increase the accommodation of wind power.

Based on the above discussion, a linear model is constructed, which can reflect these energy flow characteristics and thermal energy coupling of each module, so as to realize the operation optimization and benefit the evaluation of CHPIPs.

B. Linear Operation Model of CHPIP

The energy flow diagram of CHPIP-SACC is shown in Fig. 2. Consider the model as two parts, namely CHP subsystem and SACC sub-system. The former can be further divided into boiler combustion module, steam-cogeneration module, and regenerative heating module. These three modules can operate in coordination through steam circulation and thermal energy coupling. The latter, which consists of solar collector module, carbon capture module, and thermal storage module, is integrated into the former. Through thermal energy coupling between thermal storage module, and regenerative heating module, solar thermal energy can be effectively used for carbon capture and cogeneration operation.

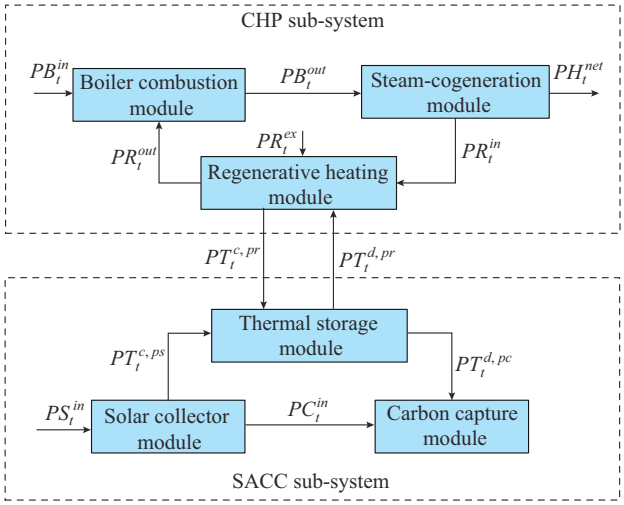

Fig. 2. Energy flow diagram of CHPIP-SACC.

Obviously, each module needs to meet the energy balance constraints and its own technical constraints. The detail is described as follows. It should be pointed out that the model in this section is used to describe the operating constraints of a single CHPIP unit. In the following system-level operation simulation optimization model, the subscript t of the relevant operation variables would be replaced with subscripts s, g, and t.

1) Operation Constraints of Solar Collector Module and Carbon Capture Module

The thermal power balance between solar collector module and the others is described in (1). Equation (2) represents the available heat collection power produced by solar concentration. The photo-thermal comprehensive conversion efficiency η^{sf} is derived from the product of solar energy receiving efficiency of solar mirrors and heat exchange efficiency of heat exchangers [28], [29]. The area of solar field S^{sf} is much smaller than that of CSP, because the solar collector module in this model is mainly used to supply energy for carbon capture instead of power generation. Constraint (3) ensures that the real input thermal power generated by solar collector module is less than the available heat collection power. Equation (4) denotes that the operation power of carbon capture module is provided by both solar collector module and thermal storage module. Equation (5) describes that the operation power of carbon capture module consists of a basic fixed power and a variable power related to the mass of captured CO_2. Different from [17], [30] that indirectly uses equivalent electric power to formulate the energy consumption of CO_2 capture, (5) directly represents the thermal power consumed for capturing CO_2. The upper and lower bounds of its operation power as well as its carbon capture rate are described in (6) and (7), respectively.

$$PS_t^{in} = PT_t^{c,ps} + PC_t^{in} \tag{1}$$

$$P_t^{sf} = \eta^{sf} S^{sf} R_t^{sf} \tag{2}$$

$$0 \le PS_t^{in} \le P_t^{sf} \tag{3}$$

$$PC_t^{op} = PC_t^{in} + PT_t^{d,pc} \tag{4}$$

$$PC_t^{op} = z_t^{op,pc} PC^B + p^C \beta_t^C e^C M_t \tag{5}$$

$$0 \le PC_t^{op} \le z_t^{op,pc} PC_{\max}^{op} \tag{6}$$

$$0 \le \beta_t^C \le \beta_{\max}^C \tag{7}$$

2) Charging and Discharging Constraints of Thermal Storage Module

Constraints (8) and (9) represent the thermal storage capacity level and its upper and lower bounds. Equation (10) ensures that the thermal storage capacity level at the ending time is equal to that at the initial time during scheduling periods. Constraints (11)-(16) impose limits of thermal storage module on charging and discharging power. Constraint (17) prevents simultaneous charging and discharging between thermal storage module and regenerative heating module, Constraint (18) plays the same role among thermal storage module, solar collector module, and carbon capture module.

$$ET_t = ET_{t-1} + \eta^c (PT_t^{c,pr} + PT_t^{c,ps})\Delta t - (PT_t^{d,pr} + PT_t^{d,pc})\Delta t / \eta^d \tag{8}$$

$$ET_{\min} \le ET_t \le ET_{\max} \tag{9}$$

$$ET_T = ET_0 \tag{10}$$

$$0 \le PT_t^{c,pr} \le z_t^{c,pr} PT_{\max}^c \tag{11}$$

$$0 \le PT_t^{c,ps} \le z_t^{c,ps} PT_{\max}^c \tag{12}$$

$$0 \le PT_t^{d,pr} \le z_t^{d,pr} PT_{\max}^d \tag{13}$$

$$0 \le PT_t^{d,pc} \le z_t^{d,pc} PT_{\max}^d \tag{14}$$

$$PT_t^{c,pr} + PT_t^{c,ps} \le PT_{\max}^c \tag{15}$$

$$PT_t^{d,pr} + PT_t^{d,pc} \le PT_{\max}^d \tag{16}$$

$$z_t^{c,pr} + z_t^{d,pr} \le 1 \tag{17}$$

$$z_t^{c,ps} + z_t^{d,pc} \le 1 \tag{18}$$

3) Energy Balance and Technical Constraints of Boiler Combustion Module and Regenerative Heating Module

Equation (19) shows that the output power of boiler combustion module, which denotes the thermal power of the main steam and the reheated steam generated by the boiler, is composed of its input power and the output power of regenerative heating module. The input power generated by combusting pulverized coal in the boiler is formulated in (20). Constraint (21) represents the minimum and maximum restrictions of the mass of pulverized coal combusted per unit time to ensure the stable operation of the boiler. The ramp-up and ramp-down rates are limited in (22). Equation (23) indicates that the steam extraction power from each stage of steam turbine would be all stored in thermal storage module. Equation (24) represents the output power of regenerative heating module, which denotes the preheating power of the feed water, is composed of thermal power of exhausted steam that has done work in steam turbine, and the discharging thermal power of thermal storage to the regenerative heating module. Constraint (25) states that the output power of regenerative heating module should be limited by the input power of boiler combustion module. This is because the boiler provides most of the energy to heat the feed water into the main steam, while the regenerative heating module only plays an auxiliary role and cannot complete this water-vapor conversion process alone [8]. It is worth mentioning that due to the dual tasks of power and heat supply of CHP units, the boilers would maintain the start-up state during the whole scheduling periods. This is why there is no constraint of start-up or shut-down state in the boiler combustion module.

$$PB_t^{in} + PR_t^{out} = PB_t^{out} \tag{19}$$

$$PB_t^{in} = \eta^{coal} q M_t \tag{20}$$

$$M_{\min} \le M_t \le M_{\max} \tag{21}$$

$$-r_{\max}^{down} \Delta t \le M_t - M_{t-1} \le r_{\max}^{up} \Delta t \tag{22}$$

$$PR_t^{in} = PT_t^{c,pr} \tag{23}$$

$$PR_t^{out} = PR_t^{ex} + PT_t^{d,pr} \tag{24}$$

$$PR_t^{out} \le \mu^{bc,in} \cdot PB_t^{in} \tag{25}$$

4) Energy Balance and Operational Constraints of Steam-cogeneration Module

Equation (26) shows that the output power of boiler combustion module, which is equal to the input power of steam-cogeneration module, is composed of the net thermal power used by steam turbine and the thermal power of extraction steam from each stage of turbine. The lower and upper bounds of the net thermal power used by steam turbine are formulated in (27). Constraint (28) relates the minimum and maximum restrictions of thermal power of exhausted steam that has done work in steam turbine, which would be used for regenerative heaters. Constraint (29) states that the steam extraction power from each stage of turbine should be limited by the output power of the boiler. Equation (30) describes the relationship between the net thermal power used by steam turbine and the electric output power of CHP units under pure condensing condition. The output power of electricity and heat under extraction condition is formulated by (31). Constraint (32) indicates that the output power of electricity and heat of CHP units is also limited by the minimum condensing working condition.

$$PB_t^{out} = PH_t^{net} + PR_t^{in} \tag{26}$$

$$PH_{\min}^{net} \le PH_t^{net} \le PH_{\max}^{net} \tag{27}$$

$$\mu_{\min}^{ex} \cdot PH_t^{net} \le PR_t^{ex} \le \mu_{\max}^{ex} \cdot PH_t^{net} \tag{28}$$

$$PR_t^{in} \le \mu^{bc,out} PB_t^{out} \tag{29}$$

$$P_t^{ConP} = \eta^{h,e} \cdot PH_t^{net} \tag{30}$$

$$P_t^{ConP} = P_t^{ExP} + c_v P_t^{ExH} \tag{31}$$

$$P_t^{ExP} - c_m (P_t^{ExH} - P_0^{ExH}) \ge 0 \tag{32}$$

III. Problem Formulation

In this section, in order to evaluate the low carbon benefits of CHPIPs in the PHIES with a high proportion of wind power during the annual operation simulation, the day-ahead economic dispatch problem is formulated by a mixed-integer linear programming model. The decision variables including the operating states of CHPIPs and the real wind power output can be determined by minimizing the expected total operation cost of PHIES. In addition, with the help of SACC, CHPIPs can provide more reserve capacity, especially the negative reserve capacity. However, it is difficult to fully calculate their available reserve capacities. Also, the previous reserve capacity calculation model is not suitable for CHPIPs, which would make their reserve capacity provision too conservative. In this paper, in order to fully measure the positive and negative reserve space provided by CHPIPs, the relevant reserve constraints of PHIES and CHPIPs have been specifically considered in the proposed model. The detailed formulation of the day-ahead economic dispatch model is described as follows.

A. Operation Optimization Model

1) Objective Function

The objective function (33) is to minimize the expected total cost of PHIES C^{total} during annual operation simulation. The expected total cost includes the operation cost of CHPIPs and the ordinary CHP units, the CO_2-related cost of the units, the penalty cost for wind and solar curtailment, the load shedding cost, as well as the penalty cost for insufficient reserve capacity.

The CO_2-related cost includes the CO_2 emission cost and the sales revenue of captured CO_2. On one hand, the operators of CHP units should purchase carbon quota from carbon trading market for CO_2 emitted directly to the atmosphere. On the other hand, the captured CO_2 can be applied for industrial production in various fields.

$$\begin{aligned}\min C^{total}=&\sum_{s\in\Omega}\sum_{t\in T}\pi_s p_s\Bigg[\sum_{g\in G}(C_g^B+\lambda^{coal}M_{s,g,t})+\\&\sum_{g\in G}\lambda_C(1-\beta_{s,g,t}^C)e_g^C M_{s,g,t}-\sum_{g\in G}\lambda_{CO_2}\eta_{CO_2}\beta_{s,g,t}e_g^C M_{s,g,t}+\\&\sum_{g\in G}\varphi_{s,cur}(P_{s,g,t}^{sf}-PS_{s,g,t}^{in})+\sum_{f\in F}\varphi_{w,cur}(P_{s,f,t}^{w,f}-P_{s,f,t}^{w,e})+\\&\varphi_{l,e,cur}P_{s,t}^{l,e,cur}+\varphi_{l,h,cur}(P_{s,t}^{l,h,r,cur}+P_{s,t}^{l,h,i,cur})+\\&\varphi_{res,cur+}R_{s,t}^{res,cur+}+\varphi_{res,cur-}R_{s,t}^{res,cur-}\Bigg]\end{aligned}\tag{33}$$

2) Operation Constraints

Equation (34) represents the supply-demand balance of electric power in the PHIES. Equation (35) represents the supply-demand balance of thermal power for residential district and industrial district in the PHIES. Equations (36) and (37) describe the active power flow of the system by using the DC power flow model. Constraint (38) represents the upper and lower bounds of the transmission capacity on each line. Constraint (39) ensures that the grid-connection power of wind generation is less than the available wind power. Constraints (40) and (41) ensure that the load shedding of electricity and heat are less than the corresponding load demand. Constraints (1) - (32) represent the linear operation model of CHPIPs formulated in Section II-B.

$$P_{s,i,t}^{w,e}+P_{s,i,t}^{ExP}=P_{s,i,t}^{l,e}-P_{s,i,t}^{l,e,cur}+P_{s,i,t}^{sp}\tag{34}$$

$$\begin{cases}\sum_{g\in G,g\in R}P_{s,g,t}^{ExH}=P_{s,t}^{l,h,r}-P_{s,t}^{l,h,r,cur}\\\sum_{g\in G,g\in I}P_{s,g,t}^{ExH}=P_{s,t}^{l,h,i}-P_{s,t}^{l,h,i,cur}\end{cases}\tag{35}$$

$$P_{s,i,t}^{sp}=\sum_{j\in i,j\neq i}P_{s,ij,t}=\sum_{j\in i,j\neq i}(\theta_{s,i,t}-\theta_{s,j,t})/x_{ij}\tag{36}$$

$$P_{s,ij,t}=(\theta_{s,i,t}-\theta_{s,j,t})/x_{ij}\tag{37}$$

$$-P_{s,ij}^{\max}\le P_{s,ij,t}\le P_{s,ij}^{\max}\tag{38}$$

$$0\le P_{s,f,t}^{w,e}\le P_{s,f,t}^{w,f}\tag{39}$$

$$0\le P_{s,t}^{l,e,cur}\le P_{s,t}^{l,e}\tag{40}$$

$$\begin{cases}0\le P_{s,t}^{l,h,r,cur}\le P_{s,t}^{l,h,r}\\0\le P_{s,t}^{l,h,i,cur}\le P_{s,t}^{l,h,i}\end{cases}\tag{41}$$

B. Reserve Capacity Model

The relevant constraints for calculating the penalty cost caused by insufficient positive and negative reserve capacities are described in detail as follows, which are composed of PHIES-related and CHPIP-related reserve constraints. The PHIES-related reserve constraints are used to calculate the total amount of reserve supply and reserve shortage in PHIES. The reserve-related variables of CHPIPs represent the states that they can reach under certain determined operation variables, when reserve capacity is performed. These variables would be restricted by CHPIP-related reserve constraints so as to fully measure the reserve space provided by units at each time.

1) Reserve Constraints for PHIES

The lower bounds of insufficient positive and negative reserve capacities are described in (42) and (43). Equation (44) represents the total amount of positive and negative reserve capacity supply in PHIES. The non-negativity of reserve capacity provided by each unit is limited by (45).

$$\begin{cases}R_{s,t}^{res,cur+}\ge R_{s,t}^{res,D+}-R_{s,t}^{res,S+}\\R_{s,t}^{res,cur-}\ge R_{s,t}^{res,D-}-R_{s,t}^{res,S-}\end{cases}\tag{42}$$

$$\begin{cases}R_{s,t}^{res,cur+}\ge 0\\R_{s,t}^{res,cur-}\ge 0\end{cases}\tag{43}$$

$$\begin{cases}R_{s,t}^{res,S+}=\sum_{g\in G}R_{s,g,t}^{res,S+}=\sum_{g\in G}(P_{s,g,t}^{ExP+}-P_{s,g,t}^{ExP})\\R_{s,t}^{res,S-}=\sum_{g\in G}R_{s,g,t}^{res,S-}=\sum_{g\in G}(P_{s,g,t}^{ExP}-P_{s,g,t}^{ExP-})\end{cases}\tag{44}$$

$$\begin{cases}R_{s,g,t}^{res,S+}\ge 0\\R_{s,g,t}^{res,S-}\ge 0\end{cases}\tag{45}$$

2) Reserve Constraints for CHPIPs

Constraint (46) restricts the ramp-up and ramp-down rates of the mass of pulverized coal that can be combusted in the boiler. Equation (47) represents the thermal storage capacity level that CHPIPs can reach at each time. Equation (48) indicates that the supply-demand balance of thermal power still

needs to be met when the reserve capacity of the units is performed. Constraints (1)~-(7)~, (9)~, (11)~-(21)~, (25)~-(32)~ impose limit on the other states that CHPIPs can reach under determined operation states when the reserve capacity has been provided. The symbol "~" denotes the reserve-related variables of CHPIPs, whose meaning is similar to the operation-related variables of CHPIPs. The serial number with the superscript "~" indicates the constraints mentioned above, in which all of the variables are replaced by the corresponding reserve-related variables.

$$-r_{\max}^{down} \le M_{s,g,t}^{\sim} - M_{s,g,t-1} \le r_{\max}^{up} \tag{46}$$

$$ET_{s,g,t}^{\sim} = ET_{s,g,t-1} + \eta^{c}(P_{s,g,t}^{c,pr\sim} + P_{s,g,t}^{c,ps\sim})\Delta t - (P_{s,g,t}^{d,pr\sim} + P_{s,g,t}^{d,pc\sim})\Delta t/\eta^{d} \tag{47}$$

$$\begin{cases} \sum\limits_{g\in G, g\in R} P_{s,g,t}^{ExH\sim} = P_{s,t}^{l,h,r} - P_{s,t}^{l,h,r,cur} \\ \sum\limits_{g\in G, g\in I} P_{s,g,t}^{ExH\sim} = P_{s,t}^{l,h,i} - P_{s,t}^{l,h,i,cur} \end{cases} \tag{48}$$

C. Abstract Formulation of Model

Based on the above discussion, the proposed mixed-integer linear model can be summarized as follows.

$$\begin{cases} \min\ (\boldsymbol{a}^{\mathrm{T}}\boldsymbol{x} + \boldsymbol{b}^{\mathrm{T}}\boldsymbol{y} + \boldsymbol{c}^{\mathrm{T}}\boldsymbol{r}) \\ \text{s.t.}\ \ \boldsymbol{P}^{\mathrm{T}}\boldsymbol{X} + \boldsymbol{Q}^{\mathrm{T}}\boldsymbol{Z} \le \boldsymbol{0} \\ \quad \boldsymbol{M}^{\mathrm{T}}\boldsymbol{X} + \boldsymbol{N}^{\mathrm{T}}\boldsymbol{Y} \le \boldsymbol{0} \\ \quad \boldsymbol{R} + \boldsymbol{X} + \boldsymbol{X}^{+} + \boldsymbol{X}^{-} \le \boldsymbol{0} \\ \quad (\boldsymbol{P}^{+})^{\mathrm{T}}\boldsymbol{X} + (\boldsymbol{E}^{+})^{\mathrm{T}}\boldsymbol{X}^{+} + (\boldsymbol{F}^{+})^{\mathrm{T}}\boldsymbol{Z}^{+} \le \boldsymbol{0} \\ \quad (\boldsymbol{P}^{-})^{\mathrm{T}}\boldsymbol{X} + (\boldsymbol{E}^{-})^{\mathrm{T}}\boldsymbol{X}^{-} + (\boldsymbol{F}^{-})^{\mathrm{T}}\boldsymbol{Z}^{-} \le \boldsymbol{0} \\ \quad \boldsymbol{Z} \in \{0,1\}, \boldsymbol{Z}^{+} \in \{0,1\}, \boldsymbol{Z}^{-} \in \{0,1\} \end{cases} \tag{49}$$

where the variable sets $\boldsymbol{x}$, $\boldsymbol{y}$, $\boldsymbol{r}$ in the objective function equal to $[M_{s,g,t}, \beta_{s,g,t}, PS_{s,g,t}^{in}]$, $[P_{s,f,t}^{w,e}, P_{s,t}^{l,e,cur}, P_{s,t}^{l,h,r,cur}, P_{s,t}^{l,h,i,cur}]$, and $[R_{s,t}^{res,cur+}, R_{s,t}^{res,cur-}]$, which are the subsets of $\boldsymbol{X}$, $\boldsymbol{Y}$, and $\boldsymbol{R}$, respectively. Set $\boldsymbol{X}$ represents the operation-related variables of units such as the input and output variables of internal modules in CHPIPs. The binary variable set $\boldsymbol{Z}$ represents the operation state of carbon capture module as well as the charging and discharging states of thermal storage module in CHPIP. The variable set $\boldsymbol{Y}$ represents the grid-connected wind power, load shedding, and power flow in PHIES. The variable set $\boldsymbol{R}$ denotes the reserve supply $R_{s,t}^{res,S+}$, $R_{s,t}^{res,S-}$ and the reserve shortage $R_{s,t}^{res,cur+}$, $R_{s,t}^{res,cur-}$ in the PHIES. The variable sets $\boldsymbol{X}^{+}$ and $\boldsymbol{X}^{-}$ denote the reserve-related variables of the units for measuring their positive and negative reserve supply, respectively. The binary variable sets $\boldsymbol{Z}^{+}$ and $\boldsymbol{Z}^{-}$ denote the states of carbon capture modules and thermal storage modules when the reserve capacity is performed, respectively. $\boldsymbol{a}$, $\boldsymbol{b}$, $\boldsymbol{c}$, $\boldsymbol{P}$, $\boldsymbol{Q}$, $\boldsymbol{E}$, $\boldsymbol{F}$ are the coefficient matrices of the corresponding variables.

The equality constraints in the model can be equivalently transformed into the inequality ones. The operation constraints $\boldsymbol{P}^{\mathrm{T}}\boldsymbol{X} + \boldsymbol{Q}^{\mathrm{T}}\boldsymbol{Z} \le \boldsymbol{0}$ and $\boldsymbol{M}^{\mathrm{T}}\boldsymbol{X} + \boldsymbol{N}^{\mathrm{T}}\boldsymbol{Y} \le \boldsymbol{0}$ include (1)-(32) and (34)-(41), respectively. The reserve constraints for PHIES $\boldsymbol{R} + \boldsymbol{X} + \boldsymbol{X}^{+} + \boldsymbol{X}^{-} \le \boldsymbol{0}$ include (42)-(45). The positive reserve constraints for CHPIPs $(\boldsymbol{P}^{+})^{\mathrm{T}}\boldsymbol{X} + (\boldsymbol{E}^{+})^{\mathrm{T}}\boldsymbol{X}^{+} + (\boldsymbol{F}^{+})^{\mathrm{T}}\boldsymbol{Z}^{+} \le \boldsymbol{0}$ are related to (46)-(48), where the superscript "~" is replaced by "+" to represent the positive reserve-related variables $\boldsymbol{X}^{+}$ and $\boldsymbol{Z}^{+}$. The negative reserve constraints for CHPIPs $(\boldsymbol{P}^{-})^{\mathrm{T}}\boldsymbol{X} + (\boldsymbol{E}^{-})^{\mathrm{T}}\boldsymbol{X}^{-} + (\boldsymbol{F}^{-})^{\mathrm{T}}\boldsymbol{Z}^{-} \le \boldsymbol{0}$ are related to (46)-(48), where the superscript "~" is replaced by "−" to represent the negative reserve-related variables $\boldsymbol{X}^{-}$ and $\boldsymbol{Z}^{-}$.

In addition, in order to unify the formulation of operation model of CHPIPs and ordinary CHP units, the CHP units can also be established with the similar constraints as CHPIPs, whose parameters related to the modules of SACC need to be set as zero.

D. Long-term Simulation Framework

In this subsection, in order to achieve a balance between accurately evaluating the low-carbon benefits of CHPIP in the PHIES during annual operation simulation and ensuring the calculation efficiency, the scenario generation model with Monte Carlo simulation [31], [32] and the scenario reduction model with *k*-means method [33], [34] are adopted to construct typical wind power scenarios and solar DNI scenarios in each season. In this paper, 16 wind power scenarios and 8 solar DNI scenarios are selected to represent the original scenarios. The detailed framework of low-carbon operation evaluation process is shown in Fig. 3. Firstly, the typical scenarios of wind power and solar DNI are constructed using the above method. Secondly, the day-ahead economic dispatch of PHIES in each scenario is determined by minimizing the expected total operation cost of PHIES with the operation constraints and reserve constraints. Finally, the economic and technical indicators are calculated based on the annual operation simulation results.

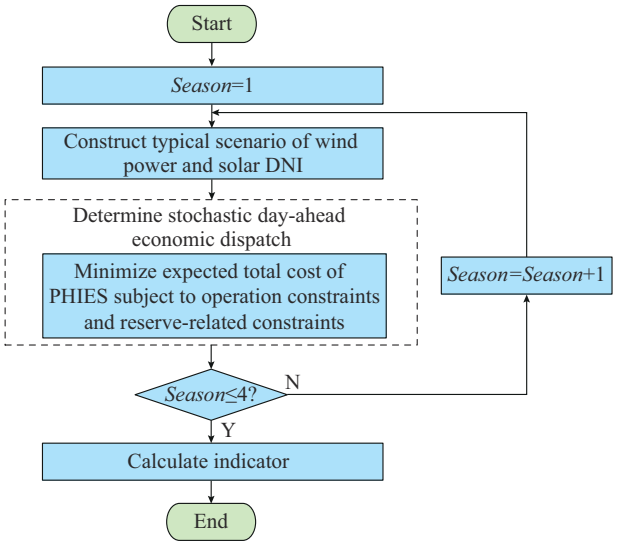

Fig. 3. Framework of low-carbon operation evaluation process.

IV. Case Study

In this section, the low-carbon benefits of CHPIPs during annual operation simulation are demonstrated based on the PHIES that contains a high share of wind power and can supply electric and thermal energy to both residential and industrial areas. All simulation cases are coded in MATLAB R2017a and are solved by a commercial optimization software called GUROBI 9.0.2.

A. Basic Data

The case studies are performed on a modified IEEE 39-bus New England test system [35] with 6 CHP units, 4 wind farmsl, and 46 transmission lines, as shown in Fig. 4. The rated installed capacity of CHP units is 150 MW. The technical and economic parameters of CHPIPs as well as ordinary CHP units are shown in Table I. There are two independent heating districts in the PHIES, where the CHP units located at buses 30 and 37 serve heat for a residential area and CHP units located at buses 31-34 supply heat for an industrial area.

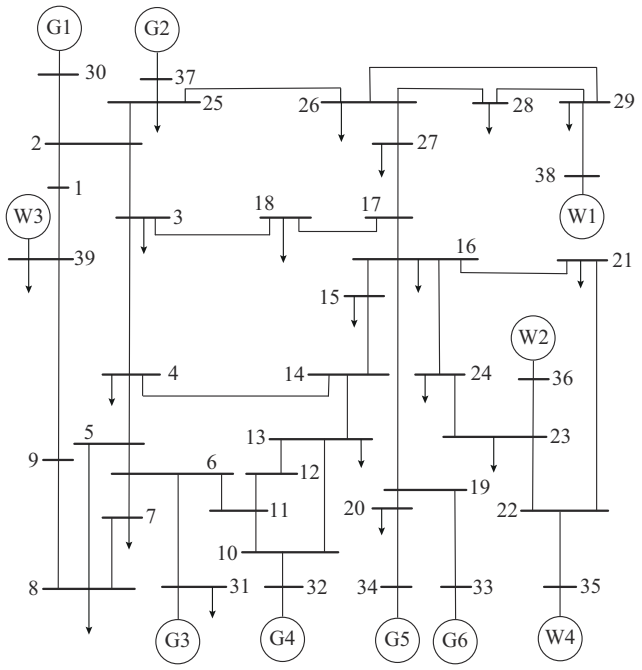

Fig. 4. Topology of modified IEEE 39-bus New England test system.

TABLE I
TECHNICAL AND ECONOMIC PARAMETERS OF CHPIPS AND ORDINARY CHP UNITS

Parameter name	Value	Parameter name	Value
η^{sf} (%)	75	η^{coal} (%)	86
S^{sf} (m^2)	240000	$M_{\min}$, $M_{\max}$ (ton/h)	30, 60
PC^B (MW)	10	$r_{\max}^{down}$, $r_{\max}^{up}$ (ton/h)	25, 25
p^C (MW/ton)	0.64	$PH_{\min}^{out}$, $PH_{\max}^{out}$	65, 385
$\beta_{\max}^C$ (%)	90	$\mu^{bc,in}$	0.392
e^C	2.32	$\mu^{bc,out}$	0.525
$P_{\max}^{op}$ (MW)	100	$\mu_{\min}^{ex}$, $\mu_{\max}^{ex}$	0.025, 0.050
η^c, η^d (%)	97.5, 97.5	c_v	0.2445
ET_0 (MWh)	150	c_m	0.6287
$ET_{\min}$, $ET_{\max}$ (MWh)	30, 300	P_0^{ExH} (MW)	26.7
$PT_{\max}^c$, $PT_{\max}^d$ (MW)	180, 180	η_{CO_2}	0.75
q (cal/g)	6395		

There are 4 geographically dispersed wind farms located at buses 35, 36, 38, and 39. The installed capacity of each wind farm is 170 MW, which makes the wind power penetration rate reach 43.0%. The forecasting error of wind power output is assumed to follow Gaussian distribution [36]. The historical data of wind power and solar power is referenced from the published data of the National Renewable Energy Laboratory (NREL) [37].

The unit price of coal is set to be 60 \$/ton. The carbon trading price and the CO_2 sale price are set to be 10 \$/ton and 1 \$/ton, respectively. The penalty factors for wind and solar curtailment are assumed to be 50 \$/MW and 20 \$/MW, respectively. The penalty factors for electric and thermal load shedding are assumed to be 1250 \$/MW and 250 \$/MW, respectively. The penalty costs for insufficient positive and negative reserve capacities are assumed to be 100 \$/MW and 10 \$/MW, respectively.

B. Operation Analysis

This subsection discusses the annual low-carbon benefits of CHPIP-SACC in the PHIES with high share of wind power. Four comparative cases are illustrated for demonstrating the operation characteristics of CHPIP-SACC in the PHIES.

1) Case 1: CHP units located at buses 30, 37 serving heat for residential area and buses 31, 32 serving heat for industrial area are integrated with SACC.

2) Case 2: CHP units located at the buses 30, 37 and buses 31, 32 are integrated with thermal storage and carbon capture module but without solar collector module.

3) Case 3: CHP units located at the buses 30, 37 and buses 31, 32 are integrated with thermal storage module but without others.

4) Case 4: none of CHP units has been retrofitted with SACC.

The results and comparison of the four cases are presented in Table II. As can be observed clearly, compared with Case 4, the annual operation benefits of PHIES in Case 1 has been significantly improved by 28.11 M\$. The reduction of CO_2-related cost has made great contributions to the improvement. On one hand, the solar thermal power provides most of the clean and renewable energy for carbon capture. On the other hand, as the benefits from carbon capture can cover the increased coal consumption cost, part of the energy for carbon capture also comes from coal combustion. Differently, as shown in Case 2, the coal combustion in the boilers supplies all of energy for carbon capture. Therefore, even if the operation of carbon capture at all costs is profitable as a whole, the expected total operation cost of PHIES is only slightly reduced by 9.83 M\$ due to the heavy operation burden of boilers. This reflects that the conventional carbon capture units without utilizing solar thermal energy would consume the massive energy from coal combustion, which is inherently uneconomical and unclean.

In Case 1 and Case 2, the wind curtailment rate and reserve insufficiency cost are both decreased to 1.48% and 1.54 M\$, respectively. This illustrates that by thermally coupling with regenerative heating module, the thermal storage module in the proposed integration scheme plays an irreplaceable role in improving the downward flexibility of CHP units. Therefore, even with the restriction of thermo-electric coupling, the minimum technical electric output of CHPIPs can still be greatly reduced through storing the thermal ener-

gy of extraction steam from each stage of turbine. Thus, the wind accommodation as well as reserve capacity, especially the negative capacity, can be substantially improved in the PHIES.

Similar to Case 4, the PHIES in Case 3 has a high carbon emission cost. However, because of the thermal storage module, the wind curtailment rate is decreased to 2.93%, thereby moderately reducing the generation operation cost and the carbon emission cost that are both caused by coal consumption. Compared with Case 1 and Case 2, the wind curtailment rate in Case 3 is 1.45% higher, while the reserve insufficiency cost in Case 3 is decreased by 0.19 M$. The reason is that during the nighttime and early morning when the wind power output is high, different operation and control strategies of thermal storage modules are adopted depending on whether carbon capture module is installed or not. In Case 1 and Case 2, during this period without sunlight, the thermal power from the extraction steam of the turbine should be stored in the thermal storage so as to supply energy for carbon capture, which also reduces the electric output of CHP units and promotes wind accommodation. While in Case 3, during the same period, thermal storage does not provide energy for carbon capture. Due to limited storage capacity to store thermal power of extraction steam, it would soon reach its maximum capacity during daytime, which restricts the minimum technical electric output of CHP units. Therefore, the wind curtailment in Case 3 is higher than those in Case 1 and Case 2. In order to alleviate this problem, some thermal storage modules choose to release their thermal energy to preheat feed water of the regenerative heating module, which in turn enhances the ability of CHP units to provide more negative reserve capacity. This is why the reserve insufficiency cost in Case 3 is lower than those in Case 1 and Case 2.

TABLE II
COMPARISON OF CASE RESULTS

Case	Total operation cost (M$)	Generation operation cost (M$)	CO_2-related cost (M$)	Load shedding (MWh)	Reserve insufficiency (M$)	Wind curtailment rate (%)	Solar curtailment rate (%)
1	172.78	155.69	14.42	0	1.54	1.48	0
2	191.06	172.57	15.81	0	1.54	1.48	
3	196.12	144.69	47.82	0	1.35	2.93	
4	200.89	145.75	48.23	0	2.33	5.95	

The simulation results of electric power operation scheduling in Cases 1 and 4 for typical scenarios with the highest probability in each season are shown in Fig. 5. Scenarios 1-4 represent four typical days in spring, summer, autumn, and winner, respectively.

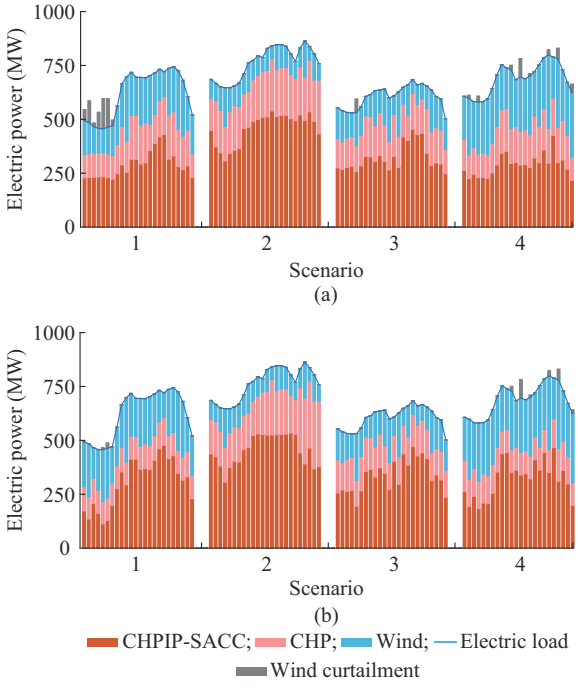

Fig. 5. Simulation results of electric power operation scheduling in Cases 1 and 4 for typical scenarios with the highest probability in each season. (a) CHP units without retrofit. (b) CHP units located at buses 30, 37 and 31, 32 integrated with SACC.

It can be observed from Fig. 5(a) that by comparing the scenarios in different seasons, due to the relatively low wind power but high electric demand, there is almost no wind curtailment in summer. While during the nighttime in other seasons, the wind power is high but the electric load space available for wind accommodation is insufficient. What is more, in order to supply enough energy for much higher thermal demand in winter and spring, the strong coupling of thermo-electric output of CHP units would restrict the reduction of their electric output. This leads to prominent wind curtailment problem. As shown in Fig. 5(b), after integrating SACC into CHP units, the wind curtailment in PHIES is decreased greatly. CHPIPs can be maintained at lower electric output under relatively high wind power condition, while the electric output of ordinary CHP units changes little. This is because the minimum electric output of a single CHPIP is reduced from 35.2% of the rated power to 13.3%.

The operation scheduling results of solar collector module and carbon capture module for a designated CHPIP in Case 1 are shown in Fig. 6 with the same typical scenarios as Fig. 5. It can be observed that there is no solar curtailment in all scenarios, because the fluctuation of solar collection power is effectively stabilized through thermal storage. Meanwhile, it is worth mentioning that with the solar collector and thermal storage supplying heat energy together, CO_2 emissions are captured as much as possible at all the time. During the daytime or the nighttime, carbon capture module is only powered by solar collector module or thermal storage module, respectively. While at the alternate moments of day and night, carbon capture module would be jointly powered by

solar collector module and thermal storage module. Due to the late sunrise time in winter, solar collector module would start to generate heat collection power approximately one hour later than other seasons. Therefore, the thermal storage module would stop assisting in carbon capture at 9 a.m. In autumn, because of weak sunlight intensity, the thermal storage module needs to start assisting in carbon capture at 3 p.m., which is about one or two hours earlier than other seasons.

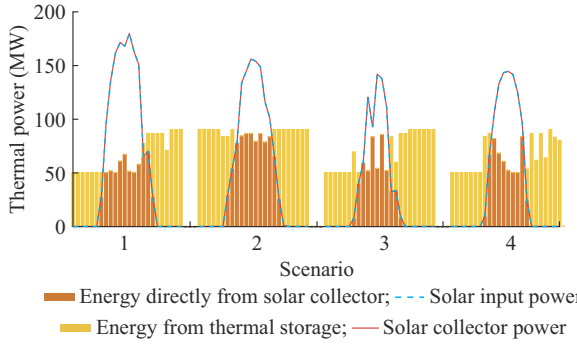

Fig. 6. Operation scheduling results of solar collector module and carbon capture module for a designated CHPIP in Case 1.

Accordingly, the operation scheduling simulation results of thermal storage module are shown in Fig. 7, in which the same designated CHPIP in Case 1 and the same scenarios are selected. As shown in Fig. 7, from the midnight to the morning, e.g., 01:00-07:00, the thermal storage capacity level shows a downward trend until reaching its minimum value. This is because when the solar collector module cannot be operated to generate solar thermal power, the thermal storage module needs to continuously release heat for carbon capture. From the morning to the afternoon, e.g., 08:00-15:00, the thermal storage capacity level shows a rapid upward trend, which reaches its maximum value at around 3 p.m. The solar collector module can generate sufficient solar thermal energy for carbon capture, the excessive part of which would be stored in the thermal storage for evening use. Due to the limited storage capacity, thermal storage would also release its redundant energy for heating the feed water of the regenerative module, so as to help the boiler reduce the coal consumption. From afternoon to evening, e.g., 16:00-21:00, the thermal storage capacity level drops rapidly. The input power of solar collector module gradually decreases to zero. Therefore, not only is there no excess energy that can be stored, but thermal storage module also has to continuously release power to support carbon capture. During the last night time, e.g., 22:00-24:00, the thermal storage capacity level gradually rises back to its initial level so as to comply with the operation constraints, which is contributed by the thermal energy of extraction steam. In addition, in order to reduce the electric output of CHPIPs and improve wind accommodation, the thermal energy of extraction steam would also be charged into thermal storage module. This is why the curve of thermal storage capacity level would form upward countertrend polylines during early morning and evening periods.

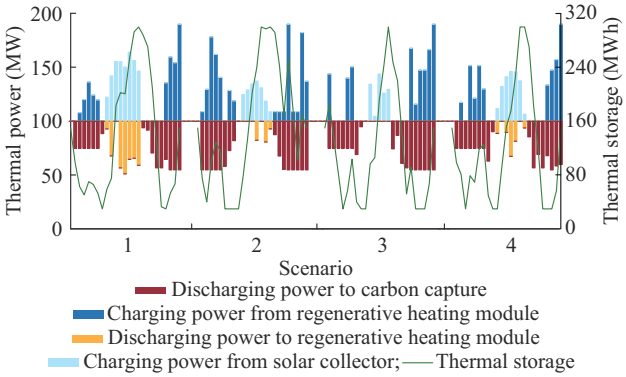

Fig. 7. Operation scheduling simulation results of thermal storage module.

C. Sensitivity Analysis

In this subsection, as shown in Fig. 8 and Fig. 9, sensitivity analysis is illustrated to study the impact of different solar field areas and different unit prices of coal on the annual operation simulation benefits of integrating SACC into CHP units located at buses 30, 37 and buses 31, 32. The solar field area for each case is shown in Table III, which determines the available solar thermal power. The unit price of coal in the cases varies from 30 $/ton to 150 $/ton, which essentially represents the ratio variations of different coal prices to the fixed carbon trading price.

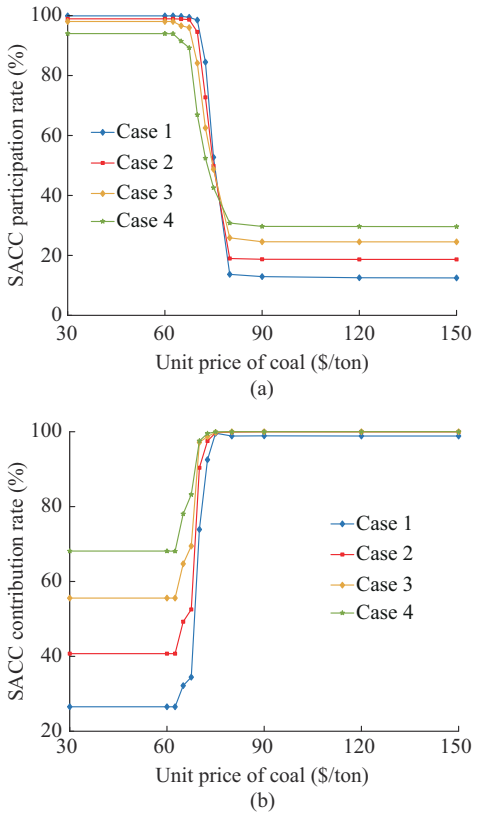

Fig. 8. SACC degree with different solar field areas and different unit prices of coal. (a) SACC participation rate. (b) SACC contribution rate.

Figure 8 shows how the SACC participation rates and the SACC contribution rates vary as the unit prices of coal increase under different solar field areas, while the variation

trends of the CO_2-related costs and the generation operation costs in the same circumstances are described in Fig. 9. The SACC participation rate denotes the ratio of energy consumption of carbon capture provided by solar thermal energy whether directly or indirectly to total available solar thermal energy throughout the year, while the SACC contribution rate represents the ratio of energy consumption of carbon capture provided by solar energy whether directly or indirectly to its total energy consumption throughout the year.

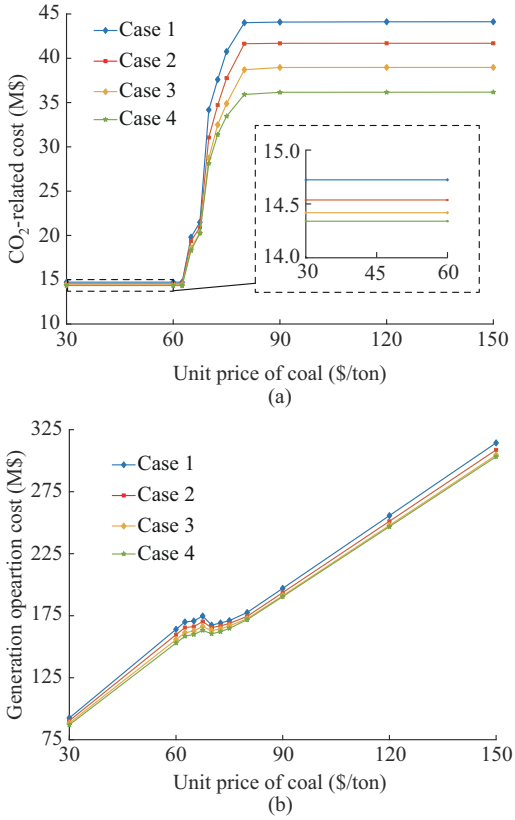

Fig. 9. Generation operation cost with different solar field areas and different unit prices of coal. (a) CO_2-related cost. (b) Generation operation cost.

TABLE III
SOLAR FIELD AREAS IN DIFFERENT CASES

Case	S^{sf} (m^2)
1	120000
2	180000
3	240000
4	300000

Actually, the thermal energy from the extraction steam of turbine that would be stored in the thermal storage is essentially derived from the increased coal consumption of boiler, which would increase the operation cost of CHPIPs. Therefore, from the perspective of the overall operational benefits of PHIES, based on the prices of coal and carbon trading quota, it is also necessary to weigh whether to supply more energy for carbon capture by increasing coal consumption. Meanwhile, there is also a certain amount of the extraction steam coming from the decreased electric output of CHPIPs in order to accommodate more wind power. The thermal energy from accommodated wind power as well as the solar thermal energy from solar collector are both valuable renewable energy. Thus, it is also important to carefully consider whether the above two types of energy are allocated to preheat the feed water so as to reduce the coal consumption, or used for carbon capture so as to reduce the purchase of carbon quota.

When the unit price of coal is lower than 65 $/ton, the ratios of coal prices and the fixed carbon trading price are relatively low, so that the benefits for carbon capture are far greater than coal saving. Thus, carbon capture module would be operated continuously at a high level, so as to capture CO_2 as much as possible. As shown in Fig. 8, since the real input solar thermal energy is almost all used for carbon capture directly or indirectly, the SACC participation rates in the cases are close to 100 %. Since it is not enough to maintain the high energy requirement of carbon capture, a large amount of thermal energy from extraction steam would help its operation. Thus, the SACC contribution rate is far less than 100%. As shown in Fig. 9, the carbon trading costs are at a very low level, while the generation operation costs rise linearly with the increase of coal price, but are still at a relatively low level.

On the contrary, when the unit price of coal is higher than 90 $/ton, the coal consumption cost becomes a prominent and decisive factor to affect the operation benefits of PHIES. CHPIPs would give priority to save coal rather than reduce CO_2 emissions, who would preferentially preheat the feed water by using the thermal energy from solar concentration and extraction steam with the help of thermal storage. As shown in Fig. 8, the SACC participation rates are at a low level, while their contribution rates are almost equal to 100%. This indicates that the extraction steam of CHPIPs almost no longer provides energy for carbon capture, which means almost all of energy for carbon capture comes from solar thermal energy. As shown in Fig. 9, the CO_2-related costs are very high, while the overall line segment of generation operation costs have shifted downward, although they still increase linearly. Under the same coal price, when the solar field area becomes larger, although the available total solar thermal energy also becomes larger, the SACC participation rate is eventually higher. This is because when the upper limit of preheating power or the maximum thermal storage capacity level is reached occasionally, much more redundant solar thermal energy would be used directly or indirectly for carbon capture so as to avoid solar curtailment.

When the unit prices of coal are between 65 $/ton and 90 $/ton, it is difficult to compare the benefits of carbon capture and coal saving. It can be observed from Fig. 8 that the PHIES faces a trade-off of energy distribution, which would rapidly tend to coal saving with the increase of coal price. Thus, the generation operation cost has appeared a countertread decline with the decrease of coal consumption rate in CHPIPs, while the CO_2-related costs increase greatly. In Fig. 9, the participation and contribution rates have also drastic variations in this transition process.

V. Conclusion

The application of solar energy as a heat source for carbon capture shows great potential to avoid massive energy consumption for coal-fired power plants during the operation of carbon capture, which also has the advantages of enhancing the operation flexibility of coal-fired power plants. In this paper, the low-carbon operation benefits of CHPIP-SACC during annual operation simulation are investigated in a PHIES with a high proportion of wind power. First, based on the selected integration scheme, the linear operation model of CHPIPs is developed considering the technical characteristics of internal modules and their thermal energy coupling interaction. Second, the day-ahead economic dispatch problem based on a mixed-integer linear programming model is presented to evaluate the expected total operation cost of PHIES during annual operation simulation, which can also fully measure the positive and negative reserve capacity provisions of CHPIPs.

The numerical simulations demonstrate that CHPIP-SACC can greatly improve the benefits of CO_2 emission reduction and reduce the generation operation cost through the effective utilization of solar thermal energy. It should be pointed out that SACC can also improve the flexibility of CHPIPs and then reduce the wind curtailment rate and reserve risk of the PHIES, which is realized by the interaction between thermal storage module and regenerative heating module. The impact of different solar field areas and different unit prices of coal on the low-carbon operation benefits of PHIES is studied in the section of sensitivity analysis. Sensitivity analysis shows the energy flow characteristics of solar thermal energy and the trade off between carbon capture and coal saving. The future work fields includes the formulation and improvement of various incentive policies for SACC technology development and CO_2 emission reduction. In the future, the technology will be more promising as the construction cost of solar field and the unit energy consumption level of carbon capture decrease.

References

[1] T. Luz and P. Moura, "100% renewable energy planning with complementarity and flexibility based on a multi-objective assessment," *Applied Energy*, vol. 255, p. 113819, Dec. 2019.

[2] S. Kiwan and E. Al-Gharibeh, "Jordan toward a 100% renewable electricity system," *Renewable Energy*, vol. 147, pp. 423-436, Mar. 2020.

[3] K. Hansen, C. Breyer, and H. Lund, "Status and perspectives on 100% renewable energy systems," *Energy*, vol. 175, pp. 471-480, May 2019.

[4] Y. Ma, Y. Yu, and Z. Mi, "Accommodation of curtailed wind power by electric boilers equipped in different locations of heat-supply network for power system with CHPs," *Journal of Modern Power Systems and Clean Energy*, vol. 9, no. 4, pp. 930-939, Jul. 2021.

[5] X. Li, D. Shi, Y. Li *et al*., "Impact of carbon regulations on the supply chain with carbon reduction effort," *IEEE Transactions on Systems, Man and Cybernetics: Systems*, vol. 49, no. 6, pp. 1218-1227, Jun. 2019.

[6] International Energy Agency. (2019, Apr.). Global energy & CO_2 status report 2019: the latest trends in energy and emissions in 2018. [Online]. Available: https://www.iea.org/reports/global-energy-co2-status-report-2019

[7] International Energy Agency. (2019, Apr.). World energy outlook 2019. [Online]. Available: https://www.iea.org/reports/world-energy-outlook-2019

[8] Y. Wang, S. Lou, Y. Wu *et al.*, "Flexible operation of retrofitted coal-fired power plants to reduce wind curtailment considering thermal energy storage," *IEEE Transactions on Power Systems*, vol. 35, no. 2, pp. 1178-1187, Sept. 2019.

[9] Y. Zhou, W. Hu, Y. Min *et al.*, "Integrated power and heat dispatch considering available reserve of combined heat and power units," *IEEE Transactions on Sustainable Energy*, vol. 10, no. 3, pp. 1300-1310, Jul. 2019.

[10] T. Zhang, W. Zhang, Q. Zhao *et al.*, "Distributed real-time state estimation for combined heat and power systems," *Journal of Modern Power Systems and Clean Energy*, vol. 9, no. 2, pp. 316-327, Feb. 2020.

[11] W. Zheng, Z. Li, X. Liang *et al*., "Decentralized state estimation of combined heat and power system considering communication packet loss," *Journal of Modern Power Systems and Clean Energy*, vol. 8, no. 4, pp. 646-656, Feb. 2020.

[12] X. Chen, C. Kang, M. O'Malley *et al.*, "Increasing the flexibility of combined heat and power for wind power integration in China: modeling and implications," *IEEE Transactions on Power Systems*, vol. 30, no. 4, pp. 1848-1857, Jul. 2015.

[13] M. Wang, A. Lawal, P. Stephenson *et al*., "Post-combustion CO_2 capture with chemical absorption: a state-of-the-art review," *Chemical Engineering Research and Design*, vol. 89, no. 9, pp. 1609-1624, Sept. 2011.

[14] C. Kale, A. Górak, and H. Schoenmakers, "Modelling of the reactive absorption of CO_2 using mono-ethanolamine," *International Journal of Greenhouse Gas Control*, vol. 17, pp. 294-308, Sept. 2013.

[15] J. Luo, X. Zhang, D. Yang *et al.*, "Emission trading based optimal scheduling strategy of energy hub with energy storage and integrated electric vehicles," *Journal of Modern Power Systems and Clean Energy*, vol. 8, no. 2, pp. 267-275, Mar. 2020.

[16] S. Reddy K., L. K. Panwar, B. K. Panigrahi *et al.*, "Modeling of carbon capture technology attributes for unit commitment in emission-constrained environment," *IEEE Transactions on Power Systems*, vol. 32, no. 1, pp. 662-671, Jan. 2017.

[17] Z. Ji, C. Kang, Q. Chen *et al.*, "Low-carbon power system dispatch incorporating carbon capture power plants," *IEEE Transactions on Power Systems*, vol. 28, no. 4, pp. 4615-4623, Nov. 2013.

[18] M. Zhao, A. I. Minett, A. T. Harris *et al.*, "A review of techno-economic models for the retrofitting of conventional pulverised-coal power plants for post-combustion capture (PCC) of CO_2," *Energy & Environmental Science*, vol. 6, no. 1, pp. 24-25, Oct. 2012.

[19] Q. Chen, C. Kang, and Q. Xia, "Modeling flexible operation mechanism of CO_2 capture power plant and its effects on power-system operation," *IEEE Transactions on Energy Conversion*, vol. 25, no. 3, pp. 853-861, Sept. 2010.

[20] F. Parvareh, M. Sharma, A. Qadir *et al.*, "Integration of solar energy in coal-fired power plants retrofitted with carbon capture: a review," *Renewable and Sustainable Energy Reviews*, vol. 38, pp. 1029-1044, Aug. 2014.

[21] C. Li, S. Guo, X. Ye *et al.*, "Performance and thermoeconomics of solar-aided double-reheat coal-fired power systems with carbon capture," *Energy*, vol. 177, pp. 1-15, Jun. 2019.

[22] F. Wang, J. Zhao, H. Li *et al.*, "Preliminary experimental study of post-combustion carbon capture integrated with solar thermal collectors," *Applied Energy*, vol. 185, pp. 1471-1480, Jan. 2017.

[23] Y. Liu, S. Deng, R. Zhao *et al.*, "Energy-saving pathway exploration of CCS integrated with solar energy: a review of innovative concepts," *Renewable and Sustainable Energy Reviews*, vol. 77, pp. 652-669, Apr. 2017.

[24] P. S. Jordan, A. M. J. Eduardo, M. C. Zdzislaw *et al*., "Techno-economic analysis of solar-assisted post-combustion carbon capture to a pilot cogeneration system in Mexico," *Energy*, vol. 167, pp. 1107-1119, Jan. 2019.

[25] M. Mokhtar, M. T. Ali, R. Khalilpour *et al*., "Solar-assisted post-combustion carbon capture feasibility study," *Applied Energy*, vol. 92, pp. 668-676, Apr. 2012.

[26] A. Qadir, L. Carter, T. Wood *et al.*, "Economic and policy evaluation of SPCC (solar-assisted post-combustion carbon capture) in Australia," *Energy*, vol. 93, pp. 294-308, Aug. 2015.

[27] O. Garbrecht, M. Bieber, and R. Kneer, "Increasing fossil power plant flexibility by integrating molten-salt thermal storage," *Energy*, vol. 118, pp. 876-883, Jan. 2017.

[28] Y. Wang, S. Lou, Y. Wu *et al.*, "Co-allocation of solar field and thermal energy storage for CSP plants in wind-integrated power system," *IET Renewable Power Generation*, vol. 12, no. 14, pp. 1668-1674, Aug. 2018.

[29] E. Du, N. Zhang, B. Hodge *et al*., "Operation of a high renewable penetrated power system with CSP plants: a look-ahead stochastic unit

commitment model," *IEEE Transactions on Power Systems*, vol. 34, no. 1, pp. 140-151, Jan. 2019.
[30] S. Lu, Y. Wu, S. Lou *et al.*, "A model for optimizing spinning reserve requirement of power system under low-carbon economy," *IEEE Transactions on Sustainable Energy*, vol. 5, no. 4, pp. 1056-1063, Oct. 2014.
[31] R. Torquato, Q. Shi, W. Xu *et al*., "A Monte Carlo simulation platform for studying low voltage residential networks," *IEEE Transactions on Smart Grid*, vol. 5, no. 6, pp. 2766-2776, Nov. 2014.
[32] H. Huang, F. Li, and Y. Mishra, "Modeling dynamic demand response using Monte Carlo simulation and interval mathematics for boundary estimation," *IEEE Transactions on Smart Grid*, vol. 6, no. 6, pp. 2704-2713, Nov. 2015.
[33] T. Xu, H. Chiang, G. Liu *et al.*, "Hierarchical *K*-means method for clustering large-scale advanced metering infrastructure data," *IEEE Transactions on Power Delivery*, vol. 32, no. 2, pp. 609-616, Apr. 2017.
[34] W. A. Omran, M. Kazerani, and M. M. A. Salama, "A clustering-based method for quantifying the effects of large on-grid PV systems," *IEEE Transactions on Power Delivery*, vol. 25, no. 4, pp. 2617-2625, Oct. 2010.
[35] M. A. Pai, *Energy Function Analysis for Power System Stability*, 1st ed. Boston: Springer, 1989.
[36] M. A. Ortega-Vazquez and D. S. Kirschen, "Estimating the spinning reserve requirements in systems with significant wind power generation penetration," *IEEE Transactions on Power Systems*, vol. 24, no.1, pp. 114-124, Feb. 2009.
[37] NREL. (2020, Jan.). Data and tools. [Online]. Available: https://www.nrel.gov/index.html

Xusheng Guo received the B.E. degree in electrical engineering from North China Electric Power University (NCEPU), Beijing, China, in 2016. He is currently pursuing the Ph. D. degree in electrical engineering in Huazhong University of Science and Technology (HUST), Wuhan, China. His research interests include power system planning and operation, renewable energy generation, carbon capture and integrated energy system.

Suhua Lou received the B.E., M.Sc., and Ph.D. degrees in electrical engineering from Huazhong University of Science and Technology (HUST), Wuhan, China, in 1996, 2001, and 2005, respectively. She is currently working as a Professor in HUST. Her research interests include power system planning, energy economics and renewable energy generation.

Yaowu Wu received the B.E., M.Sc. and Ph.D. degrees in electrical engineering from Huazhong University of Science and Technology (HUST), Wuhan, China, in 1983, 1989, and 2007, respectively. He is currently working as an Associate Professor in HUST. His research interests include power system reliability and power system operation analysis.

Yongcan Wang received the B.E. degree in electrical engineering from Sichuan University (SCU), Chengdu, China, in 2014, the Ph.D. degree in electrical engineering from Huazhong University of Science and Technology (HUST), Wuhan, China, in 2019. His research interests include power system planning and operation, renewable energy generation, coal-fired power plant flexibility retrofit and cascaded hydropower dispatch.